Biophysical Journal, Volume *113*

Supplemental Information

Membrane Curvature and Lipid Composition Synergize To Regulate N-Ras Anchor Recruitment

Jannik B. Larsen, Celeste Kennard, Søren L. Pedersen, Knud J. Jensen, Mark J. Uline, Nikos S. Hatzakis, and Dimitrios Stamou

Lipid compositions
All components are given as molar percentage.
Lipid saturation study:
POPC: POPC:POPS:DOPE-biotin:DOPE-Atto655 (88.5:9.5:1:1)
DOPC: DOPC:DOPS:DOPE-biotin:DOPE-Atto655 (88.5:9.5:1:1)

DOPE study:
0 % PE; DOPC:DOPS:DOPE-biotin:DOPE-Atto655 (88.5:9.5:1:1)
25 % PE; DOPC:DOPS:DOPE:DOPE-biotin:DOPE-Atto655 (63.5:9.5:25:1:1)
50 % PE DOPC:DOPS:DOPE:DOPE-biotin:DOPE-Atto655 (38.5:9.5:50:1:1)

Lipid length study:
DLPC: DLPC:DLPS:DOPE-biotin:DOPE-Atto655 (88.5:9.5:1:1)
DMPC: DMPC:DMPS:DOPE-biotin:DOPE-Atto655 (88.5:9.5:1:1)

We systematically change the membrane composition of the employed liposomes to correlate changes in membrane properties to altered recruitment of tN-Ras by membrane curvature. In general, changing one membrane parameter might influence others (1); nonetheless, here we will relate our observations to the major physical parameter that we change, i.e. lipid chain saturation state (POPC versus DOPC), headgroup size (DOPE), or lipid length/membrane thickness (DLPC versus DMPC). Importantly, modulating membrane curvature has been reported not to change membrane thickness (2), an observation corroborated by the molecular field calculations showing insignificant changes in membrane thickness between planar and 50 nm in diameter spherical membranes (Table S1). Also, the lipid structures in Fig. 1 B are depicted taking into account the experimentally determined values for spontaneous curvature. However, to our knowledge, only the values for DOPC and DOPE have been quantified in much detail (3-6) and for the POPC system we only found a single study (3). For DLPC we were unable to find any information on the spontaneous curvature and for DMPC it was limited to estimated values, that has not been experimentally confirmed (7, 8), although the studies do corroborate the consensus of the field that DMPC and DLPC both have positive spontaneous curvatures (9).

	Thickness (nm)			Relaxation	Calculated Bending	Experimental Bending	Spontaneous Curvature
	Planar	50 nm	% change	Ratio	Modulus (10^{-19} J)	Modulus (10^{-19} J)	nm^{-1}
DOPC	3.74	3.74	0.0	0.40	0.84	0.85 ± 0.10 (16)	-(0.05 to 0.11) (3-5)
POPC	3.7	3.69	0.3	0.28	0.80	0.77 ± 0.08 (17)	-0.022 ± 0.01 (5)
0% PE	3.74	3.74	0.0	0.40	0.85	DOPE	-(0.31 to 0.35) (4-6)
25% PE	3.74	3.74	0.0	0.40	0.85		
50% PE	3.74	3.74	0.0	0.40	0.84		
DMPC	3.44	3.43	0.3	0.35	0.71	0.69 (18)	No exp value
DLPC	3.07	3.06	0.3	0.24	0.69	0.55 (18)	No exp value

Table S1: Summary of results from the molecular field theory calculations and relevant literature values.

The concentration of DOPE-Atto655 is not biased in any curvature dependent manner

Previously we have experimentally shown that significant curvature dependent lipid demixing based on lipid spontaneous curvature does not occur in the SLiC assay through experiments with premixed pairs of fluorophores (10, 11). We tested structurally similar fluorophores, like DiD and DiO, and detected a constant average intensity ratio value as function of liposome diameter (Fig. S1 *A*) (10, 11). Even more illustrative is the similar constant intensity ratio versus liposome diameter for a DPPE-Atto633 and Palmitoyl-Fluorescein (C_{16}-F) fluorophore pair, which have vastly different intrinsic spontaneous curvatures, demonstrating no significant lipid demixing in the SLiC assay (Fig. S1 *B*) (10, 11).

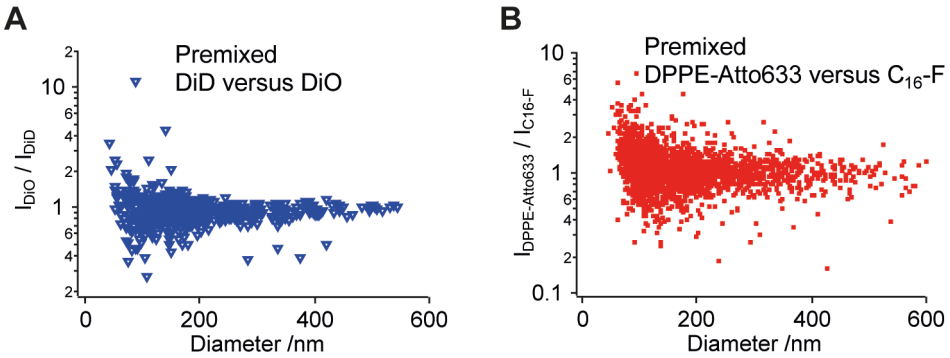

Figure S1: *A*) Intensity ratio of vesicles premixed with DiD and DiO versus vesicle diameter. *B*) Intensity ratio of vesicles premixed with DPPE-Atto633 and C_{16}-F versus vesicle diameter.

Power function fitting to extract recruitment ability

As previously described (12), we fitted the density versus liposome diameter data with an error weighted off-set power function to quantify the recruitment by membrane curvature:

$$D_{tN-Ras} = D_0 + \beta \cdot (Dia_{ves})^{\alpha} \qquad \text{(S1)}$$

with $D_{tN\text{-}Ras}$ being the peptide density, D_0 being the offset peptide density value, Dia_{ves} as the liposome diameter, and α and β representing fitting parameters. From the obtained fits we quantified the relative recruitment ratio (R), defined as the increase in peptide density when reducing the curvature by a factor of 10 (Fig. S2 and S3). R was calculated as the ratio between the density on a 40 nm and a 400 nm in diameter liposome:

$$R = \frac{dens(40\,nm)}{dens(400\,nm)} = \frac{D_0 + \beta \cdot (40\,nm)^{\alpha}}{D_0 + \beta \cdot (400\,nm)^{\alpha}} \qquad \text{(S2)}$$

We used the R values to compare the recruitment by membrane curvature of the different membrane systems. R is reported as the average ± standard error of the mean (SEM) of N independent experiments (See Fig. S3 for information on N for individual systems). We used Student's t-testing to evaluate the significance of the difference in the quantified R values and drew comparisons among various membrane systems. In Fig. S3 we assigned significance levels based on the premise: $p \leq 0.05$ (*), $p \leq 0.01$ (**) and $p \leq 0.001$ (***). We found $p = 0.00083$ for the DOPC and POPC comparison (***), $p = 0.0016$ for the DOPE 0% and the DOPE 50% comparison (**), and $p = 0.0063$ for the DMPC and DLPC comparison (**).

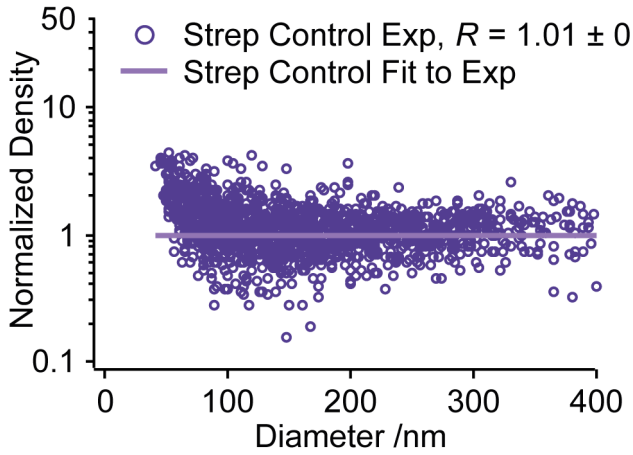

Figure S2: Negative control experiment of streptavidin binding to biotinylated liposomes showed no change in density as a function of diameter.

A

Composition	Fold increase Exp *R*	Fold increase Theory *R*	No Exp	Total No Points
DOPC	7.4 ± 0.4	8.9	9	9356
POPC	31.8 ± 6.2	36.8	8	7114
Streptavidin	1.01 ± 0.01		3	4026
0 % PE	7.4 ± 0.4	8.9	9	9356
25 % PE	6.4 ± 1.7	7.7	3	3650
50 % PE	5.1 ± 0.2	6.5	6	5330
DMPC	15.4 ± 2.9	17.7	7	3932
DLPC	31.0 ± 3.7	28.3	6	3714

B

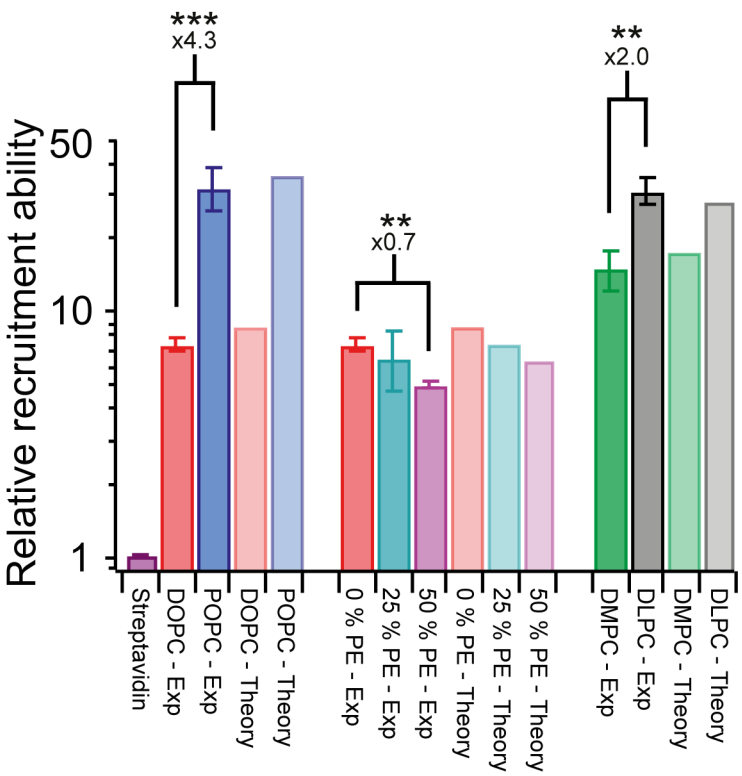

Figure S3: *A*) Summary of experimental and theoretical *R* values for all tested membrane systems. *B*) Bar chart displaying the experimental and theoretical *R* values for all tested membrane systems, including significance levels for the comparable compositions.

Calculating the average absolute tN-Ras density for specific liposome diameters

Since we acquired all data for membrane systems to be compared under identical imaging conditions, we have the ability to compare the absolute tN-Ras densities and examine how they change with liposome diameter. To do this we used the power function fit to the individual experiments, and calculated the fit function value for five different liposome diameters. We performed this operation for all experiments and calculated the average absolute tN-Ras densities and the SEM, which we present for each membrane system.

Molecular field theory for the analysis of the physio-chemical properties of model lipid membranes

A molecular field theory was used to determine the thermodynamic and structural characteristics of the lipid bilayers, providing the avenue through which a mechanistic understanding of how recruitment of tN-Ras is influenced by membrane composition and curvature. The theory explicitly incorporates the conformational energy and entropy of the hydrocarbon chains of the lipid and anchor molecules (13, 14). A description of the size and shape of each of the monomeric elements is integrated into the theory via an excluded volume constraint, representing the repulsive interactions of the molecules. Together with terms accounting for the lipid headgroups and the translational mobility of the lipids, these contributions collectively form a density functional that encompasses fluctuations over all possible states of the systems. Thermodynamic information may be acquired by accessing the equilibrium states of the system, represented by the set of functions that embody the overwhelmingly most probable configurational arrangements sampled by the molecules. Acquisition of this set of functions is achieved through functional minimization with respect to the system's free variables.

The pure-component model membranes under consideration were spherical vesicles, consisting of DOPC, POPC, DLPC, and DMPC. Lipid molecular areas calculated for the planar geometries were 0.695 nm^2/molecule, 0.672 nm^2/molecule, 0.627 nm^2/molecule, and 0.621 nm^2/molecule, respectively (Table 1). These calculations were performed at 295K for DOPC and POPC. On account of DMPC's high transition temperature, DMPC bilayer calculations were performed at 305K to ensure a liquid disordered phase state. DLPC bilayers were also analyzed at 305K to make a direct comparison to the likewise fully saturated, but longer chained DMPC bilayers. All calculated molecular areas are in excellent agreement with experimental findings (15). Membrane thickness was evaluated under tensionless equilibrium conditions. The effects of membrane curvature on bilayer thickness were found to be negligible (Table S1), as expected.

Each of these lipid species have two hydrophobic tails built from a distinct number of hydrocarbon units that are either single-bonded, as with fully saturated DLPC and DMPC, or mono-unsaturated with a cis double-bond in one (POPC) or both (DOPC) lipid tails. The length and degree of unsaturation of each of the tails governs their accessible spatial orientations. These conformations are specified exactly, using Flory's Rotational Isomeric States Model (16), in which each successive monomer along a single chain may assume one of three possible orientations with respect to the bond-angle it forms with its predecessor. These dihedral angles are *gauche plus (+)* at 120º, *gauche minus (-)* at -120º, and *trans*, which forms a plane perpendicular to the interface at 0º. The two *gauche* conformations are thermally excited states, which exist in energy wells that confer stability to these orientations;

both contribute an increase in the internal energy by ε = 500 cal/mole (16). The *trans* conformation is of the lowest energy level and is regarded as a reference state with zero energy contribution. For a comprehensive representation of the entire configurational sample space within the bilayer, we performed a series of Euler rotations on each conformation accessed by the acyl chains about the bilayer normal.

The lipid vesicle's N total number of lipids is divided between the two leaflets of the bilayer. The fractions of lipids in the inner and external leaflets are denoted x_I and x_E, respectively, and are equal to 0.5 in symmetric, planar bilayers. Molecular rearrangement ensues from curving the bilayer, altering the lipid fraction in each leaf; larger curvatures provoke more lipid translocation from the compressed internal leaf to the expanded external leaf. As such, the total area parallel to the midplane (the x-y plane) of the bilayer is a function of both the curvature and the location (along the z-axis) between the two leaflets. We define the z-axis to be perpendicular to the membrane interfaces with its origin at the midplane. The total lateral area at a distance, z, within the hydrophobic core is given by

$$A(z,\mathbf{c}) = A(0)\left[1 + (C_1 + C_2)z + C_1C_2z^2\right] \qquad \text{(S3)}$$

where C_1 and C_2 are the principal curvatures, defined as $C_i = 1/R_i$; R_i are the radii of curvature to the bilayer midplane, and $A(0)$ is the midplane area.

The intermolecular repulsions are modeled as excluded volume interactions that are introduced as a packing constraint on the density functional. The molecular theory is solved under the constraint that the total density of the hydrophobic region is a constant (i.e. that it is incompressible). The constant density constraint implies that the average molecular area, $a(z) = A(z)/N$, *occupied* by the molecules in any layer within the hydrophobic core must be equal to the average *available* molecular area. That is,

$$a(z,\mathbf{c}) = \sum_i \sum_\delta x_i x_{i\delta} n_i^{tails} \left\langle v_{i\delta}(z) \right\rangle \qquad \text{(S4)}$$

for $-l < z < l$. $\left\langle v_{i\delta}(z) \right\rangle$ are the ensemble-averaged contributions to the volume of the hydrophobic core from molecule i and the subscript δ stands for I or E, specifying the inner or external bilayer leaf, respectively.

Terms delineating the energetic and entropic inputs to the system are explicitly written into the functional. The incompressibility constraint is enforced by the Lagrange multipliers, $\beta\pi(z,\mathbf{c})$, which come to physically represent the lateral pressure profile of the bilayer's hydrophobic region upon functional minimization. Minimization yields an expression for the probability of each of the molecular configurations as a function of the imposed constraints, namely, the lateral pressure. All thermodynamic parameters of interest, as well as molecular level architectural detail within our model membranes, are accessible from the consequent minimized function arising as the system's thermodynamic potential:

$$\frac{\beta W}{N}=\beta\gamma_0\left\{a(0)\left[1+\left(\frac{x_{PC}a_{PC}+x_{PE}a_{PE}}{a(0)}\right)^2\right]\right\}+\sum_i\sum_\delta x_i x_{i\delta}\ln\left(\frac{x_i x_{i\delta}\lambda_i^2}{a(0)e}\right)$$
$$+\sum_i\sum_\delta\sum_{\alpha_{i\delta}}\left\{n_i^{tails}x_i x_{i\delta}\left[P_{i\delta}(\alpha_{i\delta})\left(\ln(P_{i\delta}(\alpha_{i\delta}))+\beta\varepsilon(\alpha_{i\delta})\right)\right]\right\} \qquad \text{(S5)}$$
$$+\int_{-l}^{l}\beta\pi(z,\mathbf{c})\left\{\sum_i\sum_\delta x_i x_{i\delta}n_i^{tails}\left\langle v_{i\delta}(z)\right\rangle-a(z,\mathbf{c})\right\}dz,$$

where $\beta = 1/k_BT$ and λ is the thermal wavelength of the molecule. A molecule's configuration is denoted α_δ,; $\varepsilon(\alpha_\delta)$ is the internal energy of the lipid chains defined by the number of gauche bonds existing in configuration α_δ. The first term on the right-hand side of the above equation relates the contributions of the lipid headgroups using Tanford's opposing force model (17). These contributions include the interfacial energy generated by the area of the polar headgroups in contact with water in terms of the bare oil-water surface tension $\gamma_0 = 0.12k_BT/\text{Å}^2$, and the steric penalty, or repulsion, incurred from close packing. Since PC and PE headgroups are of different sizes, the repulsion term is weighted by the mole fractions of each headgroup present. We take the two repulsive parameters to be $a_{PC}=36\text{Å}^2$/molecule and $a_{PE}=30\text{Å}^2$/molecule. The second term reflects the effect on the free energy from the translation of the lipids. The third term describes the conformational energy and internal energy of the chains and the fourth term encompasses the excluded volume repulsive interactions that are accounted for by the incompressibility constraint.

The probability distributions of the lipid chains are dependent on the molecular configurational states and the degree of curvature of the bilayer. The latter dependency is explicitly governed by the lateral pressure profile within the hydrophobic channel, conferred by the field-variables $\pi(z,\mathbf{c})$. These probability distributions, solved for via functional minimization, are given by the following expression:

$$P_{i,\delta}\left(\alpha_{i,\delta},\mathbf{c}\right)=\frac{1}{q_{i,\delta}(\mathbf{c})}\exp\left\{-\beta\varepsilon(\alpha_{i,\delta})-\int_{-l}^{l}\beta\pi(z,\mathbf{c})v_{i,\delta}(z,\alpha_{i,\delta})dz\right\} \qquad \text{(S6)}$$

$q_{i\delta}(\mathbf{c})$ is the single molecule partition function (normalization of the probability) defined as:

$$q_{i\delta}(\mathbf{c})=\sum_{\alpha_{i,\delta}}\exp\left\{-\beta\varepsilon(\alpha_{i,\delta})-\int_{-l}^{l}\beta\pi(z,\mathbf{c})v_{i,\delta}(z,\alpha_{i,\delta})dz\right\} \qquad \text{(S7)}$$

Any curved bilayer experiences an asymmetry of stress as the lipids in the exterior leaflet relax due to expansion above the midplane and as the lipids in the interior leaflet compress below the midplane. A chemical potential gradient between the bilayer leaflets is immediately established upon bending, causing lipids from the interior leaflet to diffuse to the outer leaflet to reduce the imposed stresses and chemical potential imbalance. In reference (13) we used the molecular theory to show that the amount of lipid flip-flop

between the leaflets has considerable influence on the physical properties on a curved bilayer. We introduced a term called the relaxation ratio, $\eta = \frac{2}{l}\left(\frac{\partial x_E}{\partial C_+}\right)$, where C_+ is the sum of the principle radii of curvature. We take the relaxation ratio to be constant for all curvatures with respect to a particular lipid system, so the exterior mole fraction can be determined by the following expression for spherical vesicles:

$$x_E(R) = 0.5000 + \frac{l\eta}{R} \qquad \text{(S8)}$$

The relaxation ratio for each bilayer system was determined by fitting the theoretical bending modulus to those measured by experiment. Comparison of the calculated bending moduli to experimental values are listed in Table S1 (18-21).

Calculating the Lateral Pressure Profile from the Molecular Theory

The molecular theory provides a direct route to calculating the lateral pressure profile. The lateral pressure, Π, is defined to be the transverse component of the pressure tensor minus the normal component of the pressure tensor (22-24). The lateral pressure is related to the surface tension, γ, for any geometry through the following expression (25):

$$\gamma = \int_{-\infty}^{\infty} \left[P_N(z,\mathbf{c}) - P_T(z,\mathbf{c})\right] dz = -\int_{-\infty}^{\infty} \Pi(z,\mathbf{c}) dz \qquad \text{(S9)}$$

The mathematical expression for the surface tension can be obtained for the molecular theory by taking the area derivative of the free energy expression (S5):

$$\beta\gamma(T,A,N,\mathbf{c}) = -\left\{\frac{1}{a(0)} - \beta\gamma_0\left[1 - \left(\frac{x_{PC}a_{PC} + x_{PE}a_{PE}}{a(0)}\right)^2\right] + \int_{-l}^{l} \beta\pi(z,\mathbf{c}) dz\right\} \qquad \text{(S10)}$$

In order to relate equations (S9) and (S10) together we need to split the domain up into three regions. The first domain is from $-\infty$ to $-l$, and this makes up the internal aqueous phase and the headgroups of the lipids that make up the inner leaflet. The second domain is from l to ∞, and this makes up the volume occupied by the headgroups of the lipids in the outer leaflet and the exterior aqueous phase. The third domain is from $-l$ to l and this domain is the region occupied by the hydrophobic fatty-acid chains of the lipids. Utilizing these three domains, the lateral pressure profile can be written as follows:

$$\begin{aligned} &\int_{-\infty}^{-l} \beta\Pi^{\text{interior}}(z,\mathbf{c}) dz + \int_{l}^{\infty} \beta\Pi^{\text{exterior}}(z,\mathbf{c}) dz + \int_{-l}^{l} \beta\Pi^{\text{hydrophobic}}(z,\mathbf{c}) dz = \\ &\frac{1}{a(0)} - \beta\gamma_0\left[1 - \left(\frac{x_{PC}a_{PC} + x_{PE}a_{PE}}{a(0)}\right)^2\right] + \int_{-l}^{l} \beta\pi(z,\mathbf{c}) dz \end{aligned} \qquad \text{(S11)}$$

where the lateral pressure profile has been split into a sum over the three domains. The sum of the integrals over the first and second domain of the lateral pressure are equal to the sum

of the contribution of the headgroups and translational free energy of the lipids to the surface tension. The integral over the third domain of the lateral pressure is equal to the integral over the Lagrange multiplier. Mathematically, this is expressed as the following:

$$\int_{-\infty}^{-l} \beta\Pi^{\text{interior}}(z,\mathbf{c})dz + \int_{l}^{\infty} \beta\Pi^{\text{exterior}}(z,\mathbf{c})dz = \frac{1}{a(0)} - \beta\gamma_0\left[1-\left(\frac{x_{PC}a_{PC}+x_{PE}a_{PE}}{a(0)}\right)^2\right] \quad \text{(S12)}$$

$$\int_{-l}^{l} \beta\Pi^{\text{hydrophobic}}(z,\mathbf{c})dz = \int_{-l}^{l} \beta\pi(z,\mathbf{c})dz$$

where we see the connection between the lateral pressure and the Lagrange multiplier for the molecular theory being that they are equal inside the hydrophobic region of the lipid bilayer.
A universal characteristic of every lateral pressure profile calculated from the molecular theory in this work is that the value is zero at the midplane. We will therefore call $\beta\pi(z,\mathbf{c})$ the relative lateral pressure, since the value at each position z in the hydrophobic region is relative to the value at the midplane ($z=0$).
It is important to note the differences when comparing the lateral pressure profiles determined by the molecular theory used in this manuscript to those obtained by simulations (22-24). The lateral pressure profiles for lipid bilayers obtained by simulation all share three basic structural characteristics: 1) the value of the lateral pressure is zero far enough away from bilayer to be in the bulk aqueous domain, 2) the lateral pressure plunges to negative values in the headgroup region, and 3) the lateral pressure oscillates with an overall positive value inside the hydrophobic region (the sum of the lateral pressure inside the hydrophobic region is positive to offset the negative values in the headgroup region). The same three characteristics are conserved with the profiles obtained by the molecular theory. The headgroup regions give a net negative value that is balanced by the positive values in the hydrophobic region in order to give a zero surface tension for each bilayer studied in this manuscript. The differences between the lateral pressure profile obtained by theory and simulation inside of the hydrophobic region is due to the differences in the way the profile is calculated. With the molecular theory, the translational free energy and the contribution of the headgroups are decoupled from the contributions made by the fatty-acid tails. The simulations do not separate these contributions; however, the accounting of the overall thermodynamics of bilayer system is equivalent within the approximations made in the theory. In other words, if the simulation and theory use the same level of course-graining and the correlations were fully accounted for in the molecular theory, then the results would be identical from the point of view of the thermodynamics of the system. The reason for the difference in shape of the local lateral pressure profile is due to the contributions of the lateral pressure profiles being separated with the theory.

Theoretical protein recruitment to model lipid membranes as a function of membrane curvature

When a bulk solution of proteins with chain anchors is in contact with a curved lipid bilayer, thermodynamics requires that the chemical potential of the chain anchor, μ_A, must be equal in the bulk and bilayer phases:

$$\mu_A^{bulk} = \mu_A(\mathbf{c}) \quad \text{(S13)}$$

The chemical potential of the chain anchors can be determined by the potential-distribution theorem (14, 26). For our molecular theory, the areal density of the proteins for a given curvature, normalized to the areal density of the proteins for a planar bilayer, is written as:

$$\frac{\rho_A(\mathbf{c})}{\rho_A(\mathbf{c}=\mathbf{0})} = \frac{\prod_{k=1}^{n} q_{k,E}(\mathbf{c})}{\prod_{k=1}^{n} q_{k,E}(\mathbf{c}=0)}, \qquad \text{(S14)}$$

where $\rho_A(\mathbf{c})$ is the exterior aerial density of the proteins as a function of curvature. The products in this expression depend on the type of anchor motif, ranging over the partition functions, $q_k(\mathbf{c})$, corresponding to each anchor molecule associated with the membrane-recruited protein. The partition functions are unique for each type of chain anchor (for example, the 16-carbon fully saturated palmitoyl and the 12-carbon tri-unsaturated, branched farnesyl chain anchors associated with N-Ras). The structural variations in the chain anchors engender a distinct set of accessible configurational states to each, motivating the differences in their partition functions. By observing equation (S7), the dependency of the partition function on the lateral pressure is explicit. It is clearly illustrated theoretically that lipid anchor adsorption is regulated by the particular pressure profile assumed by the hydrophobic region of the bilayer, subject to the mediating factors of temperature, composition, and curvature (Fig. S3 and S4). Such a mechanism for protein recruitment to curved membranes is substantiated by the good agreement demonstrated between the calculated and experimental results for protein recruitment within a variety of lipid membranes by curvature.

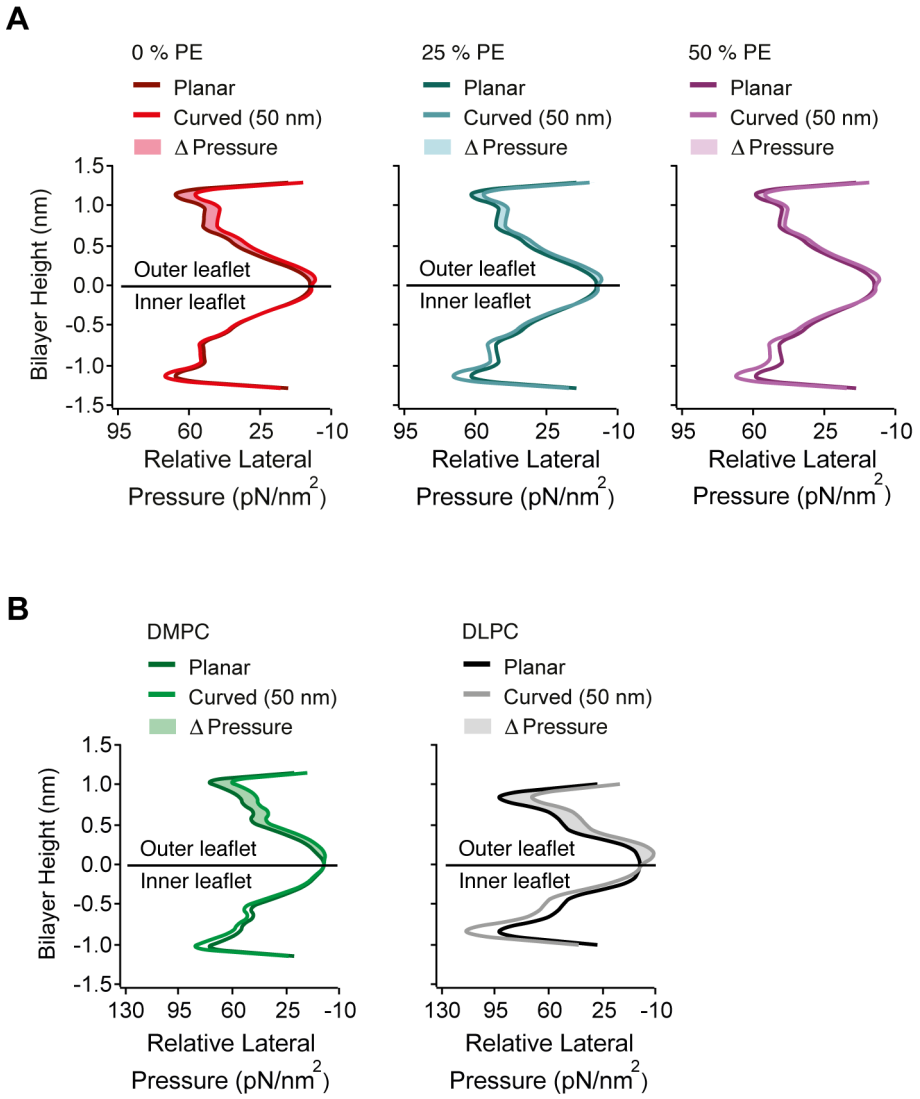

Figure S4: *A*) Theoretically calculated relative lateral pressure profiles along the bilayer normal for the hydrophobic region of 0 % PE, 25 % PE and 50 % PE membranes. The top part represents the outer monolayer (outer leaflet), the bottom represents the inner monolayer (inner leaflet) of the membrane and the relative lateral pressure profile is depicted for either planar (dark line) or curved (pale line, 50 nm diameter liposome) membranes. The curvature-dependent relief in the relative lateral pressure of the outer monolayer, ΔP, is calculated as the total area between the curves (shaded area). *B*) Theoretically calculated relative lateral pressure profiles along the bilayer normal for the hydrophobic segment of DMPC (green) and DLPC (black).

It is important to note that some curvature sensing proteins, e.g. N-BAR domains, are known to operate at a high surface coverage and introduce significant membrane deformation (27), however, the theoretical calculations in this work implicitly assume that the binding of tN-Ras does not lead to membrane deformation. This assumption should be valid since we have previously shown that lipidated moieties bind at a low surface coverage (<5 %) and do not induce visible changes in membrane morphology (12, 28). This indicates that the binding of tN-Ras does not significantly alter the lateral pressure. An important corollary from the

theoretical model, however, is that any other extrinsic parameters affecting membrane lateral pressure will lead to altered tN-Ras recruitment. This could be the binding and subsequent scaffolding of other peripheral proteins, the lateral segregation of transmembrane proteins, or interactions between the membrane and the cell cytoskeleton. All would provide the cell with additional means to tune the local density of lipidated proteins and provide feed-back regulation through the modulation of the lateral pressure profile.

Strong correlation between *R* values and the curvature dependent % change in lateral pressure

To further try to elucidate the underlying biophysical mechanism for the curvature- and compositional dependent recruitment of tN-Ras we extracted the % change in either the area per lipid or the lateral pressure when curving the membrane from flat to 50 nm. We plotted these values against the experimentally determined R values and even though the relative differences in the curvature dependent % change in the area per lipid between different membrane systems are small we still see a tendency towards a larger % area change resulting in a higher *R* value (Fig. S5 *A*). A much stronger tendency was seen for the curvature dependent % change in lateral pressure, a value for which we see a larger difference between the different membrane systems and which displays an almost linear dependence with the *R* values for the whole range of pressure changes (Fig. S5 *B*). This very strong correlation further substantiates modulations of the lateral pressure as the underlying mechanism for the compositional and curvature mediated recruitment of tN-Ras.

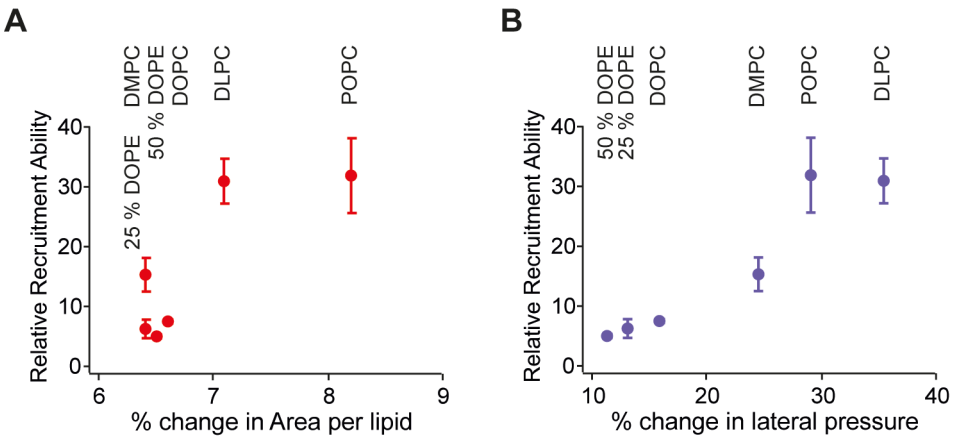

Figure S5: *A*) Experimentally determined *R* values versus the theoretically calculated curvature dependent % change in the area per lipid. *B*) Experimentally determined *R* values versus the theoretically calculated curvature dependent % change in the lateral pressure.

Supporting References

1. McIntosh, T. J., and S. A. Simon. 2006. Roles of bilayer material properties in function and distribution of membrane proteins. Annu. Rev. Bioph. Biom. 35:177-198.
2. Kucerka, N., J. Pencer, J. N. Sachs, J. F. Nagle, and J. Katsaras. 2007. Curvature effect on the structure of phospholipid bilayers. Langmuir 23:1292-1299.
3. Kollmitzer, B., P. Heftberger, M. Rappolt, and G. Pabst. 2013. Monolayer spontaneous curvature of raft-forming membrane lipids. Soft Matter 9:10877-10884.
4. Kooijman, E. E., V. Chupin, N. L. Fuller, M. M. Kozlov, B. de Kruijff, K. N. J. Burger, and P. R. Rand. 2005. Spontaneous curvature of phosphatidic acid and lysophosphatidic acid. Biochemistry 44:2097-2102.
5. Zimmerberg, J., and M. M. Kozlov. 2006. How proteins produce cellular membrane curvature. Nat. Rev. Mol. Cell Biol. 7:9-19.
6. Kamal, M. M., D. Mills, M. Grzybek, and J. Howard. 2009. Measurement of the membrane curvature preference of phospholipids reveals only weak coupling between lipid shape and leaflet curvature. Proc. Natl. Acad. Sci. 106:22245-22250.
7. Orsi, M., J. Michel, and J. W. Essex. 2010. Coarse-grain modelling of DMPC and DOPC lipid bilayers. J. Phys.-Condes. Matter 22.
8. Marsh, D. 2007. Lateral pressure profile, spontaneous curvature frustration, and the incorporation and conformation of proteins in membranes. Biophys. J 93:3884-3899.
9. Strandberg, E., D. Tiltak, S. Ehni, P. Wadhwani, and A. S. Ulrich. 2012. Lipid shape is a key factor for membrane interactions of amphipathic helical peptides. BBA - Biomembranes 1818:1764-1776.
10. Larsen, J., N. S. Hatzakis, and D. Stamou. 2011. Observation of Inhomogeneity in the Lipid Composition of Individual Nanoscale Liposomes. J. Am. Chem. Soc. 133:10685-10687.
11. Elizondo, E., J. Larsen, N. S. Hatzakis, I. Cabrera, T. Bjornholm, J. Veciana, D. Stamou, and N. Ventosa. 2012. Influence of the preparation route on the supramolecular organization of lipids in a vesicular system. J. Am. Chem. Soc. 134:1918-1921.
12. Larsen, J. B., M. B. Jensen, V. K. Bhatia, S. L. Pedersen, T. Bjørnholm, L. Iversen, M. Uline, I. Szleifer, K. J. Jensen, N. S. Hatzakis, and D. Stamou. 2015. Membrane curvature enables N-Ras lipid anchor sorting to liquid-ordered membrane phases. Nat. Chem. Biol. 11:192-194.
13. Uline, M. J., and I. Szleifer. 2013. Mode specific elastic constants for the gel, liquid-ordered, and liquid-disordered phases of DPPC/DOPC/cholesterol model lipid bilayers. Faraday Discuss. 161:177-191.
14. Uline, M. J., G. S. Longo, M. Schick, and I. Szleifer. 2010. Calculating Partition Coefficients of Chain Anchors in Liquid-Ordered and Liquid-Disordered Phases. Biophys. J 98:1883-1892.
15. Poger, D., and A. E. Mark. 2010. On the Validation of Molecular Dynamics Simulations of Saturated and cis-Monounsaturated Phosphatidylcholine Lipid Bilayers: A Comparison with Experiment. J. Chem. Theory Comput. 6:325-336.
16. Flory, P. J. 1969. Statistical Mechanics of Chain Molecules. Wiley-Interscience, New York.
17. Israelachvili, J. N. 1991. Intermolecular and Surface Forces. Academic Press, Elsevier.

18. Rawicz, W., K. C. Olbrich, T. McIntosh, D. Needham, and E. Evans. 2000. Effect of chain length and unsaturation on elasticity of lipid bilayers. Biophys. J 79:328-339.
19. Arriaga, L. R., I. Lopez-Montero, F. Monroy, G. Orts-Gil, B. Farago, and T. Hellweg. 2009. Stiffening Effect of Cholesterol on Disordered Lipid Phases: A Combined Neutron Spin Echo plus Dynamic Light Scattering Analysis of the Bending Elasticity of Large Unilamellar Vesicles. Biophys. J 96:3629-3637.
20. Kucerka, N., Y. F. Liu, N. J. Chu, H. I. Petrache, S. Tristram-Nagle, and J. F. Nagle. 2005. Structure of fully hydrated fluid phase DMPC and DLPC lipid bilayers using X-ray scattering from oriented multilamellar arrays and from large unilamellar vesicles. Biophys. J 88:245A-245A.
21. Dimova, R. 2014. Recent developments in the field of bending rigidity measurements on membranes. Adv. Colloid Interface Sci. 208:225-234.
22. Gullingsrud, J., and K. Schulten. 2004. Lipid bilayer pressure profiles and mechanosensitive channel gating. Biophys. J 86:3496-3509.
23. Sodt, A. J., R. M. Venable, E. Lyman, and R. W. Pastor. 2016. Nonadditive Compositional Curvature Energetics of Lipid Bilayers. Phys. Rev. Lett. 117.
24. Orsi, M., and J. W. Essex. 2013. Physical properties of mixed bilayers containing lamellar and nonlamellar lipids: insights from coarse-grain molecular dynamics simulations. Faraday Discuss. 161:249-272.
25. Rowlinson, J. S., and B. Widom. 1982. Molecular Theory of Capillarity. Dover Publications, New York.
26. Widom, B. 1982. Potential-distribution Theory and the Statistical-mechanics of Fluids. J. Phys. Chem. 86:869-872.
27. Peter, B. J., H. M. Kent, I. G. Mills, Y. Vallis, P. J. G. Butler, P. R. Evans, and H. T. McMahon. 2004. BAR domains as sensors of membrane curvature: The amphiphysin BAR structure. Science 303:495-499.
28. Hatzakis, N. S., V. K. Bhatia, J. Larsen, K. L. Madsen, P. Y. Bolinger, A. H. Kunding, J. Castillo, U. Gether, P. Hedegard, and D. Stamou. 2009. How curved membranes recruit amphipathic helices and protein anchoring motifs. Nat. Chem. Biol. 5:835-841.